Zoological Journal of the Linnean Society (1986), *87*: 181–214 With 52 figures

Development, structure and function of rhinoceros enamel

ALAN BOYDE

Department of Anatomy and Embryology, University College London, Gower Street, London WC1E 6BT

AND

MIKAEL FORTELIUS

Department of Geology, University of Helsinki, Snellmaninkatu 5, SF-00170 Helsinki, Finland

Received March 1985, accepted for publication May 1985

Vertical enamel prism decussation in the inner-layer enamel of rhinoceroses occurs as the result of vertical translation, in opposite senses, of rows of ameloblasts, which begins very shortly after amelogenesis commences at the enamel-dentine junction. Prisms in the centre of the decussating zones are stacked in the Pattern 2 arrangement. Zone boundary prisms adopt intermediate orientations, are locally nearly perpendicular to the enamel surface, and have a cylindrical, Pattern 1 cross-section. Decussation also continues in the outer-layer enamel, but the prisms all have occlusal-going courses: the occlusal-going zones of the inner enamel continue as the more occlusally oriented zones of the outer layer. Abrasion resistance to diamond polishing and soft abrasive projectile erosion (air-polishing with $NaHCO_3$) and resistance to ion beam erosion is greater with distance from the nearest prism boundary discontinuity. Polished surface areas containing longitudinally sectioned prisms are more prone to 'air-polishing' and 'arbonding' erosion than areas with transversely sectioned prisms. These observed relationships fully explain the relief developed at natural wear surfaces.

KEY WORDS:—Rhinoceros – enamel – prisms – decussation – development – structure – function – wear.

CONTENTS

Introduction 182
Materials 183
Rhinoceroses 183
Comparisons with other groups 183
Methods 183
Light microscopy 183
Tandem scanning reflected light microscopy 183
Sample finishing procedures for mature teeth 185
Preparation of developmental material for SEM 187
Scanning electron microscopy 189

0024-4082/86/060181+34 $02.00/0

Results 191
Previous work 191
Development and structure in *Ceratotherium simum* 193
Wear 205
Discussion 208
Vertical decussation 208
Wear 210
Acknowledgements 212
References 213
List of abbreviations 213

INTRODUCTION

Hunter–Schreger bands are zones in dental enamel in which the prisms have a common orientation property which contrasts with that in adjacent zones. In the great majority of mammals these bands are nearly parallel with the formative margin of the enamel during its development, and are thus also parallel with the incremental features seen at the completed tooth surface known as the perikymata. The bands are thus zones in which the prims pass to either left or right in their passage from the enamel dentine junction (EDJ) to the tooth surface. The prisms usually have a net inclination towards the occlusal direction in the tooth and are not confined to single zones. The zones, however, represent a single set of directions for the prisms within them.

In many mammalian fossils, including at least members of the extinct orders Pantodonta, Dinocerata, Embrithopoda and Astrapotheria, and in fossil and recent rhinocerotoids (families Hyracodontidae, Rhinocerotidae and Amynodontidae), the Hunter–Schreger bands are dispersed vertically along the tooth, at right-angles to the direction of progression of formation. Prisms thus decussate vertically, and this vertical decussation appears to begin at the EDJ (Rensberger & Koenigswald, 1980; Rensberger, 1983; Fortelius, 1984). Development of prism decussation involves the relative translatory movement of the enamel formative cells, the ameloblasts, across the surface of their secretory product, the enamel (Woll, 1942; Boyde, 1964, 1967, 1969). The normal direction of decussation involves one band of cells moving towards the left as well as occlusal, the next towards the right and the next alternate zone to the left, etc. For vertical decussation to occur, we would presume that such bands of ameloblasts would translate along the longitudinal tooth axis. If, however, we consider the situation for the first enamel increment which forms on the dentine mould in the tooth germ, it will be seen that there is no enamel for the cells to move across, unless, indeed, the presecretory preameloblasts were engaged in such relative movement. The main reason for undertaking this study was therefore, in the first instance, to establish how vertical decussation begins at the EDJ.

The movement of ameloblasts involved in the development of prism decussation can be inferred and deduced from the morphology of the developing enamel surface. We have, therefore, examined the details of the commencement of vertical decussation by studying early stages of enamel deposition in fetal rhinoceroses.

The worn occlusal surfaces of rhinoceros teeth show grooves and ridges which correspond with the vertical prism decussation zones. This underlying microscopic structure must therefore have a functional significance, at least in that it generates a partly serrated biting surface. We have examined the details

of the microscopic arrangement of the enamel prisms in mature adult teeth and attempted to correlate the wear properties of the teeth with the enamel structure, making observations on both natural wear surfaces and artificially abraded surfaces cut in a variety of directions with respect to the underlying structure.

MATERIALS

Rhinoceroses

Ceratotherium simum

Fragments of upper mature deciduous (DM_3, paracone) and permanent (M_3, protocone) molars. Dry specimens from BM(NH), unregistered. The right hemimandible of one fetus, initially frozen, but the tissue later preserved in 10% neutral formol saline. Several upper deciduous tooth germs from another fetus, with 2–3 cm of calcified tissue already formed. These were preserved and transported in 70% ethanol (Figs 1, 3–27, 29–34, 45).

Diceros bicornis

One nearly complete first upper molar (BM(NH) 36.9.1.1) and several smaller fragments of dry permanent teeth (Figs 2, 38–44, 46–50).

Coelodonta antiquitatis

Upper molar fragments BM(NH) unregistered. Kent's Cavern, Pleistocene (Fig 28).

Comparisons with other groups

Developing enamel was obtained from the South American tapir, *Tapirus terrestris* (Fig. 52), and the camel, *Camelus dromedarius* (Fig. 51). Mature enamel samples were prepared from tapir, horse, camel and cow enamel.

METHODS

Light microscopy

Sections of *Ceratotherium simum* DM_3 ectoloph and M_3 protoloph as well as *Diceros bicornis* M_1 ectoloph were cut in the longitudinal, 45° and transverse planes, all perpendicular to the tooth surface and the EDJ. Transverse sections at 45°, 80°, 90° and 135° to the EDJ (included angle towards cervical) and longitudinal sections at 45° to the EDJ were also prepared. These sections were mounted in balsam, and examined in ordinary transmitted light, and between crossed polars. Measurements were made of the apparent angles between prisms in adjacent zones and of the angles with respect to the EDJ, the enamel surface and the incremental line direction in the enamel (Fig. 1).

Tandem scanning reflected light microscopy

We used a new version of the tandem scanning reflected light microscope described by Petran *et al.* (1968) to study the enamel structure in the sub-surface

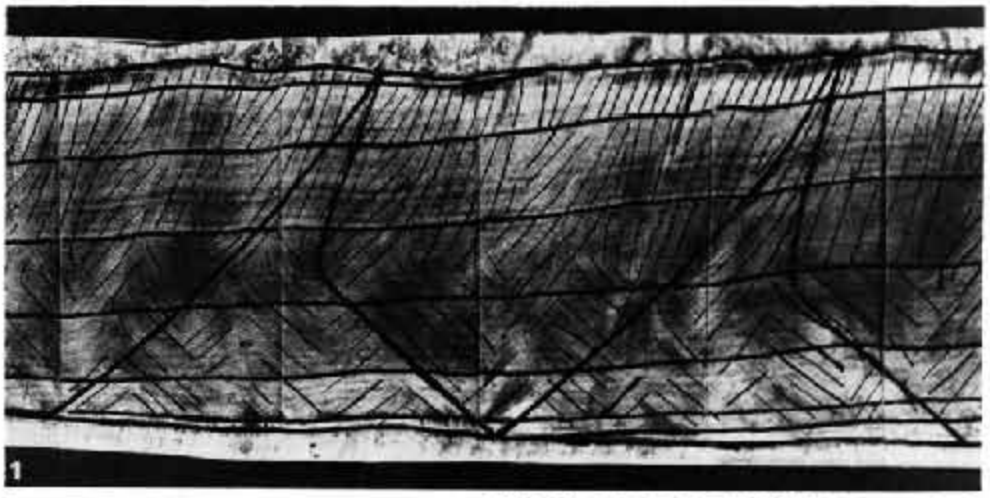
1


2

deep to both natural and artificial tooth surfaces. Using water, or oil-immersion objectives we were able to determine either the prism cross-section and/or the prism direction in thin layers up to 200 μm deep to the surface of the entire tooth specimen (Fig. 2).

Sample finishing procedures for mature teeth

Polishing

Facets prepared in directions parallel to the tooth surface, LS, TS and 135° TS etc., were prepared by hand-grinding small blocks against successively finer, wet abrasive papers, then polished on diamond-paste-coated laps using 6 μm and 1 μm diamond (Figs 6, 7, 46, 28, 29).

Very small shaped specimens

Cylindrical rod-shaped specimens of 500 μm were cut using a 1 mm diameter, 40-bladed tungsten carbide finishing burr in a dental air-turbine handpiece, using the burr perpendicular to the tooth surface and leaving the rod projecting from the EDJ. Square-section rods of 200 μm diameter were produced in the inner enamel (at the depth of the most marked prism decussation) using the burr to cut parallel to the EDJ and leaving a block made entirely of enamel and supported by the superficial enamel. These samples were H_3PO_4 etched to reveal the prism details (Figs 24, 25).

Vector polishing

Carefully oriented blocks were polished avoiding any rotation of the sample during the 6 and 1 μm diamond polishing stages, so that the abrasive vector (in a different sense from that of Rensberger & Koenigswald, 1980) was known and marked on the SEM specimen stub. The generation of defects as a consequence of the direction of unidirectional diamond polishing could thus be examined (Figs 40, 41).

Phosphoric acid etching

Polished enamel surfaces were etched with either 0.5% H_3PO_4 for 45, 60 or 90 s or with 1% H_3PO_4 for 30 s. These regimes can be expected to remove a total of about 1 μm tissue (Boyde, Jones & Reynolds, 1978: figs 20–27).

'Airbrasion' air-propelled hard abrasive

We abraded oriented, polished enamel facets using the SS White Industrial Abrasive Unit (The SS White Dental Mfg. Co., E 40 St., New York, NY,

Figures 1–5. Fig. 1. Photograph of montage of ordinary transmitted light micrographs of a longitudinal section of white rhinoceros deciduous molar, DM_2, ectoloph with superimposed tracing of some incremental lines and some sections of prism courses. In addition, the total course of four prisms is reconstructed in heavy outline. Dentine below, cement above. Enamel thickness 1200 μm. Fig. 2. Tandem scanning reflected light micrograph of oblique transverse section of black rhinoceros permanent molar ectoloph. Whiter areas have prisms more parallel with plane of section. Note that the darkest zones of the inner enamel turn into whitest zones in transitional region. Dentine below, enamel surface above. Enamel thickness 2000 μm. Fig. 5. Reflected light photograph of developing enamel surface in white rhinoceros deciduous molar prepared as a gold-coated SEM specimen. Illumination from one direction at oblique incidence produces high contrast in alternate occlusal- and cervical-going zones. Print from Ektachrome colour transparency. Field width approx. 4000 μm.

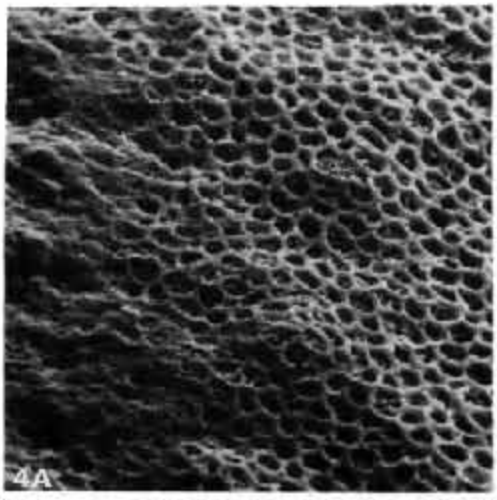
4A

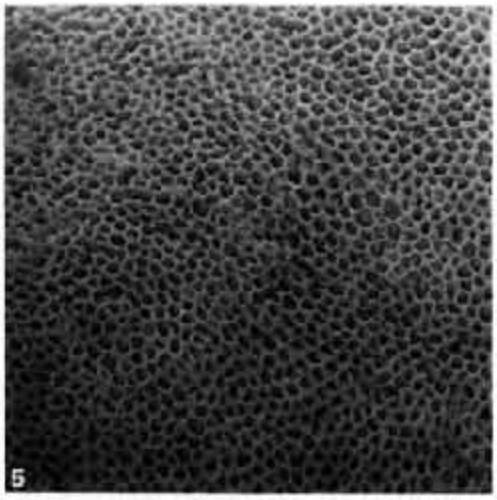
5

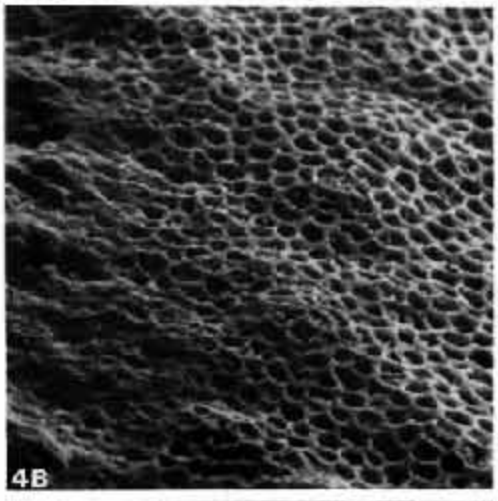
4B

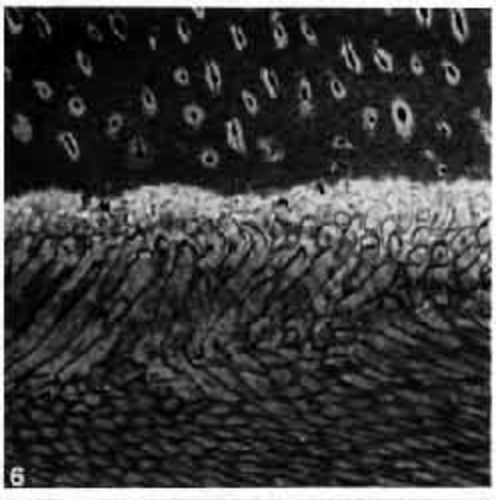
6

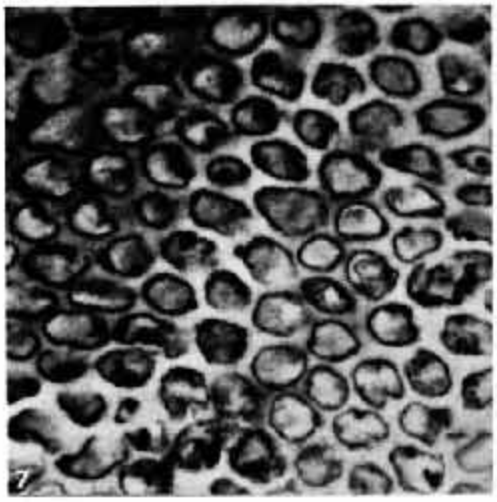
7


8

U.S.A.). Alumina of 10 μm particle size was used with a 500 μm diameter cylindrical nozzle, 80 p.s.i. (5 bar) air pressure at 3 mm working distance for 1–10 s. Since this procedure leaves a surface which is deeply pocked at the scale of enamel prisms, the airbraded surfaces were etched with 1% H_3PO_4 for 30 s to reveal the underlying prism orientations (Figs 42–45).

'Air-polishing'—air-propelled soft abrasive

In this technique the abrasive powder is sodium bicarbonate. This is propelled by a 5 bar air stream through 600 μm diameter nozzle. This gas jet is shrouded by a concentric water jet, which limits the spread of the dry abrasive, which is, of course, soluble in water. The equipment used was the Dentsply/Cavitron Prophy-Jet (Dentsply International, York, PA 17405, U.S.A.). Treatment times of 60 s at 2–3 mm working distance were used as standard, covering an area of 4 mm^2 uniformly within the period. Much shorter periods could be used with considerable effect (Figs 47–50).

Ion etching—micromilling

Using an Edwards High Vacuum IBMA 1 ion beam machining apparatus (Edwards High Vacuum, Manor Royal, Crawley, Sussex, England), diamond-polished samples cut parallel to the tooth surface and the EDJ in the inner enamel were eroded with a 50–70 μA beam of 5 keV Ar^+ ions, 15° beam incidence angle, under constant rotation, for periods of 15–30 min at a vacuum of 0.15 mbar. This regime again removes less than 1 μm tissue (Fig. 28).

Microhardness testing

Diamond-polished surfaces were subjected to microhardness indentation testing using a Vickers indenter, and test loads of 10, 20, 50, 100 and 200 g. Hardness values were calculated from measurements made by either optical microscopy or SEM (Fig. 46).

Preparation of developmental material for SEM

The hard parts within the deciduous molar tooth germs were dissected free of surrounding tissues, dehydrated in ethanol, substituted with $C_2Cl_3F_3$ and critical-point dried (CPD) from CO_2 (Fig. 4). A new dehydration and $C_2Cl_3F_3$ substitution procedure was also developed for these teeth, in which the ethanol

---

Figures 4–8. Fig. 4A,B. White rhinoceros fetal mandibular deciduous molar tooth germ. Stereopair showing first enamel development on EDJ. Note the uneven topography caused by the rough surface of the dentine at the future EDJ. SE. Field width 78 mm Fig. 5. White rhinoceros fetal mandibular deciduous molar tooth germ. Field occlusal to the zone of symmetrical shallow pits closest to the junction as shown in Fig. 4A,B. The majority of these pits face towards cervical (below) and show prism boundary cracks which are open towards occlusal side. SE. Field width 1.38 μm. Fig. 6. Longitudinal section of EDJ in white rhinoceros upper deciduous molar tooth germ, embedded in PMMA and polished on fine sandpaper. Note the hypermineralized layer of enamel at the EDJ and the formation of peritubular zones in the dentine. Silver-coated BSE image. Field width 198 μm. Fig. 7. Tangential section close to EDJ in white rhinoceros lower deciduous molar, carbon-coated, BSE image. Field width 46 μm. Fig. 8. Tangential section passing through EDJ in white rhinoceros permanent molar, air-polished and gold coated. The air-polishing etches out the occlusal-facing zones showing where their orientations change with respect to the EDJ. BSE-ET. Field width 3750 μm.

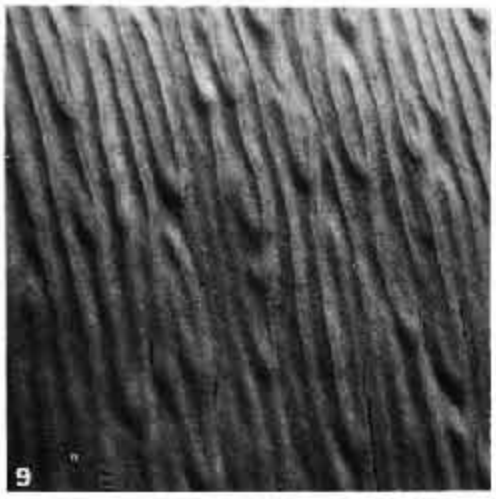
9

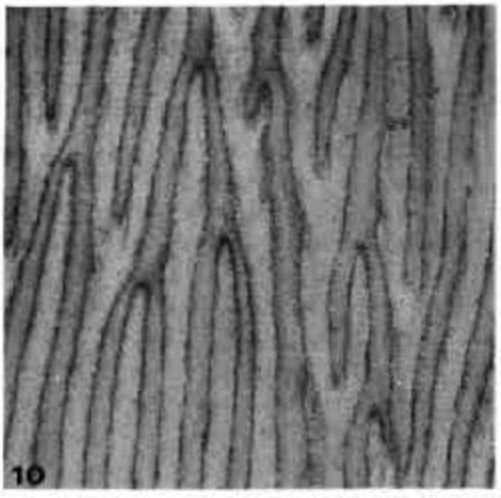
10

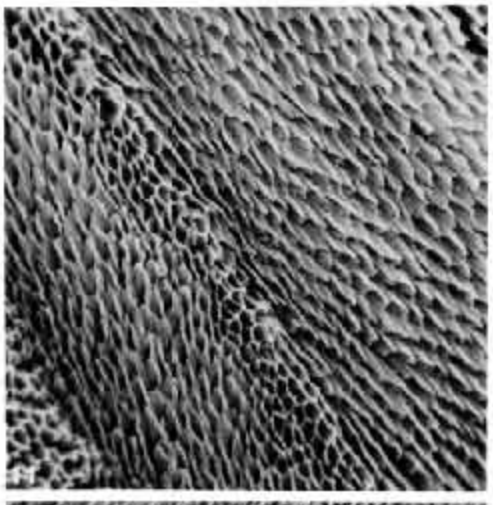
11


12

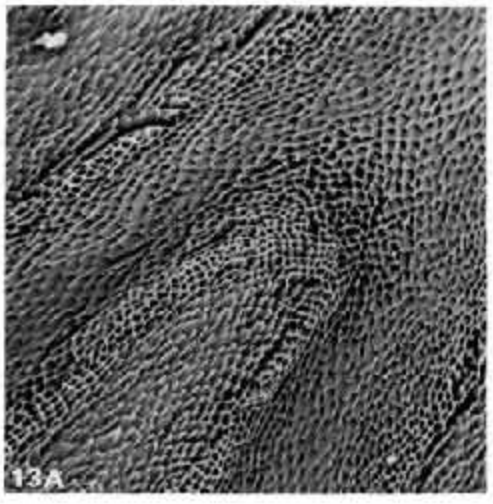
13A

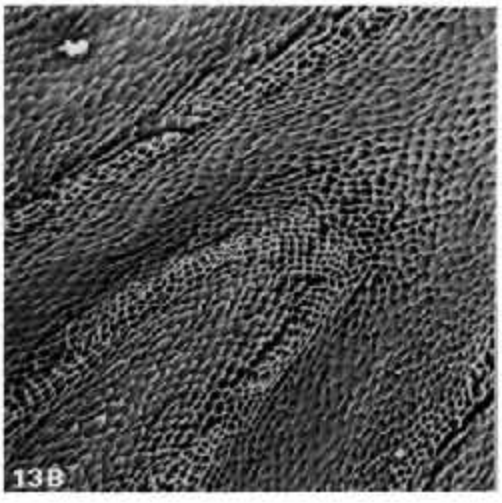
13B

and $C_2Cl_4F_2$ were refluxed in a Soxhlet apparatus before transfer to the CPD bomb: the details of procedure are given by Boyde & Tamarin (1984).

Some of the CPD samples were oxygen-plasma ashed to remove the residual enamel organ debris and incidentally the non-mineralized predentine matrix, thus exposing the mineralizing front of the dentine and enamel (Boyde & Martin, 1982; Figs 5, 9–13, 30–36).

Further samples were made anorganic by treatment with a NaOCl solution, followed by washing with water and either freeze-drying from water, or critical-point drying as described above.

The best results qualitatively, though necessarily limited in scope, were obtained by plasma ashing PMMA-embedded fetal tooth samples (Figs 14–19; Boyde & Martin, 1982).

Scanning electron microscopy

Coating

SEM samples were sputter coated with Au or Au–Pd, or coated with carbon (Figs 6, 7, 29, 38–41, 46) by evaporation before examination in Cambridge Stereoscan SEMs, marks 1 and S4-10.

Imaging modes

SE: Secondary electron imaging at 10 kV beam voltage, the sample tilted towards the collector (Figs 4, 5, 14–19, 28, 43, 51, 52).

CBSE: Converted backscattered electron imaging at 20 kV beam voltage, using the same SE detector, but with the samples biased at +200 V to prevent the escape of SE. This mode produces high topographic contrast and overcomes problems due to sample charging (Boyde & Cowham, 1980; Figs 42, 43, 45, 47).

BSE: Backscattered electron imaging with a four-sector solid state detector and a 20 kV beam, the sample, where possible, at normal incidence to both the beam and the detector. If the signals from opposing detector quadrants are summed, density dependence in the image is optimized, as for example, in imaging prism boundaries in polished or ion-etched surfaces with very little topographic contrast (Figs 4, 5, 10–13, 20–37, 39–41, 44, 46, 48–50).

BSE A–B: If opposing quadrant signals are subtracted the resulting image is most strongly dependent on topography, very useful, for example, in examining the low topography developed by short periods of 'air-polishing' (Fig. 9).

BSE-ET: Backscattered electron imaging with the conventional Everhart Thornley biased scintillator detector with the grid bias switched to

---

Figures 9–13. Fig. 9. BSE A–B image. Topographic contrast due to relief of decussating zones in CPD, plasma-ashed inner enamel of white rhinoceros fetal deciduous molar tooth germ. Cervical towards top. Field width 4238 μm. Fig. 10. BSE image of similar field, cervical to top. Whiter zones are occlusal-going, greyer zones are cervical-going, black margins are zone boundaries in this contrast mode. Field width 2000 μm. Fig. 11. BSE image of white rhinoceros reflux CPD, plasma-ashed, developing enamel surface of inner zone, showing occlusal- and cervical-going zones and 'symmetrical' pits facing nearly perpendicular to the surface at a zone boundary. Field width 100 μm. Fig. 12. Near normal incidence view (BSE 20 kV) of reflux, CPD, plasma-ashed white rhinoceros DM_3 showing contrast in orientation of occlusal- and cervical-going zones, and near surface normal orientation on zone boundary pits. Note the concentration of preparative cracks in the zone boundary region. Field width 180 μm. Fig. 13A,B. Same preparation, cervical to top right, showing a Y-junction. Stereo viewing shows the zone border at the end of the cervical-going zone to be proud of the surrounding surface of the occlusal-going zone which is divided to make the Y-formation. Field width 202 μm.

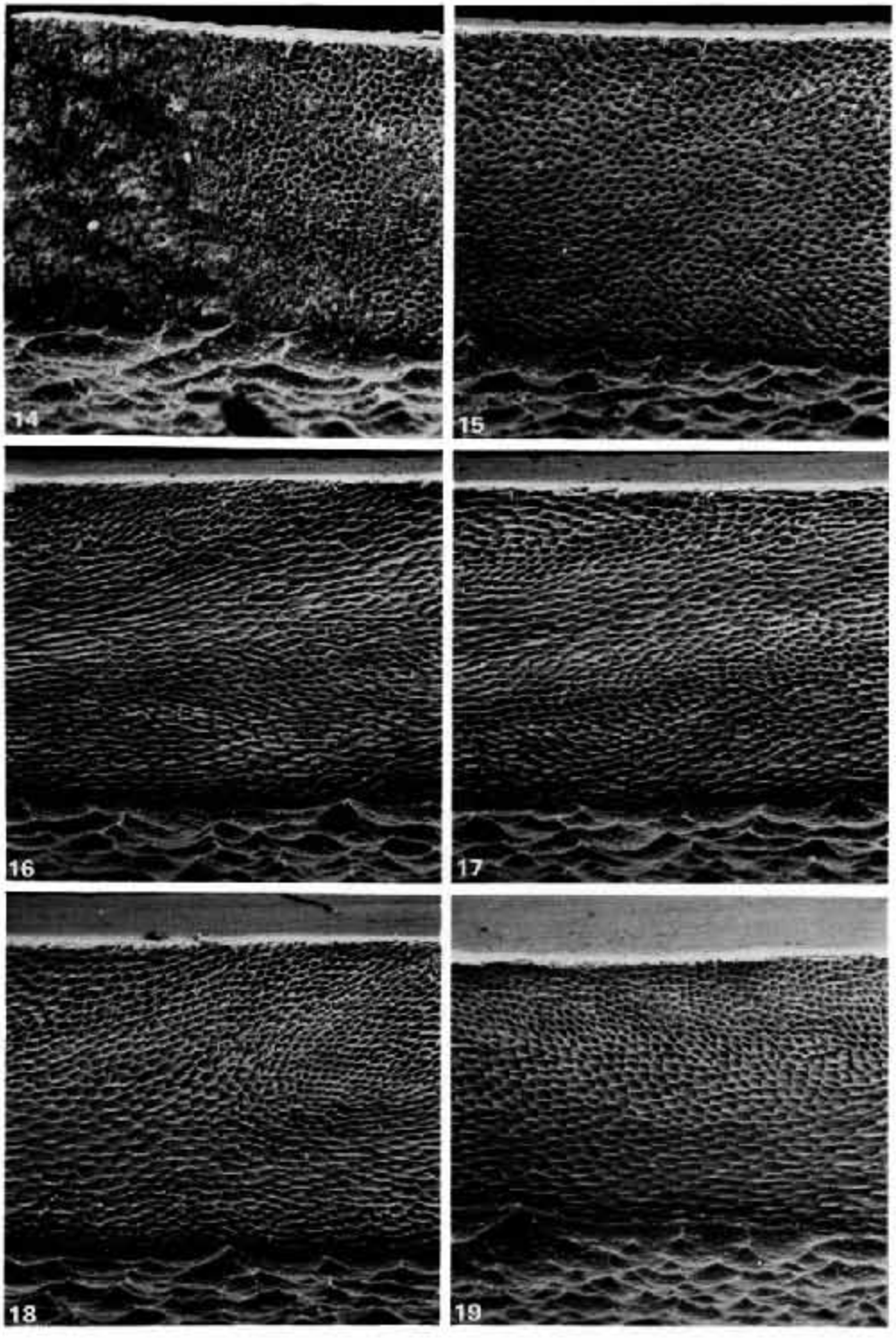
14
15
16
17
18
19

– 50 V to prevent secondary electrons, with energies of less than 50 eV, from reaching the detector: such BSE-ET images are then made with line of sight backscattered electrons, again showing high topographic contrast (Fig. 8).

STEREO: Stereo images were obtained by beam tilting so that three-dimensional orientations could be appreciated and studied directly without photographic recording (Cambridge Stereoscan S1 modified as described by Boyde 1974). Recorded stereo-pair images were taken by tilting the specimen 8 10° between two exposures (Cambridge Stereoscan S4-10: Figs 4, 13, 24, 25, 44).

RESULTS

Previous work

In their important pioneering study, Rensberger & Koenigswald (1980) showed that Hunter Schreger bands in the inner half (or more) of the enamel of rhinoceroses are vertically disposed. Their model showed the inner layer prisms lying at up to 45° to the enamel–dentine junction and the mature surface, equally but oppositely oriented in the cervically and occlusally inclined zones. They concluded that the prisms in the outer enamel do not decussate, but that they lie *either* parallel with the prisms in the occlusal-going inner zones (Hunter–Schreger bands), in which case the cervical-going inner layer prisms bent through 90° at the border between the inner, vertically decussating, and the outer, non-decussating layers; *or* that the outer prisms all lay in an orientation intermediate between those of the inner cervical- and occlusal-going prisms. This they figure as being perpendicular to the mature surface (Rensberger & Koenigswald, 1980: fig. 14). Implicit in their diagrams is the assumption that prisms begin to decussate immediately at the enamel–dentine junction.

As regards the relationship of this structure to wear in function, Rensberger & Koenigswald (1980) concluded that the inner layer decussating zones explained the ridges which develop on the worn enamel. They described two sets of ridges, which they called A and B, the B ridges developing close to the enamel–dentine junction and the A ridges also developing in the inner decussating layer just inside the transition to the outer layer. They explained these two types or location of ridge in terms of the direction and angle of an 'abrasive vector' meeting the plane of the wear surface. According to their model the enamel displays maximum resistance to wear when the prisms are parallel with the abrasive vector.

The foregoing summary of the major points made by these previous authors will explain our concentration upon certain features of our new results.

Figures 14–19. Series of pictures from a montage of a longitudinal section through PMMA-embedded white rhinoceros DM_1 upper tooth. Montage covers width of region exposed by plasma ashing for 48 h. Fig. 14 shows first enamel on dentine at the cervical end of the tooth. Fig. 15, two field widths occlusally, shows more pits facing cervically. Fig. 16, five more widths occlusally, and Fig. 17, five more fields occlusally again, both show the typical scenery encountered everywhere in inner enamel development with occlusal- and cervical-going zones separated by zone boundaries with pits facing perpendicular to the surface. Figs 18 & 19, respectively five and 11 more field widths occlusally, show similar features, but a Y-junction node can be seen in Fig. 18. SE. Field widths are 186 μm.

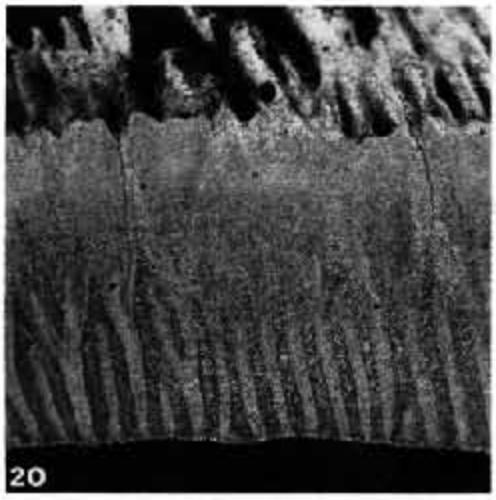
20

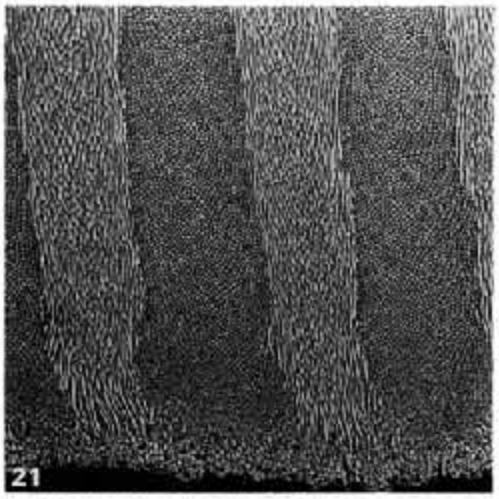
21

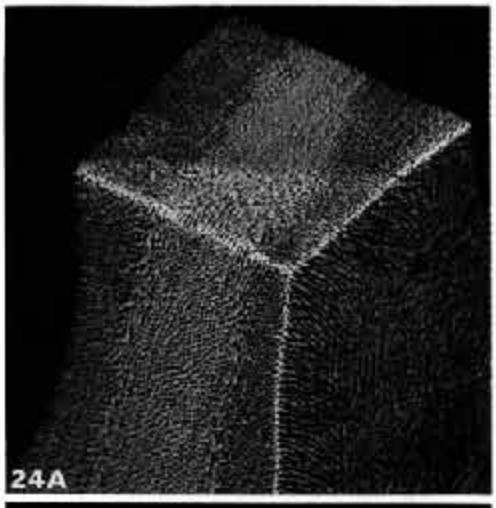
24A

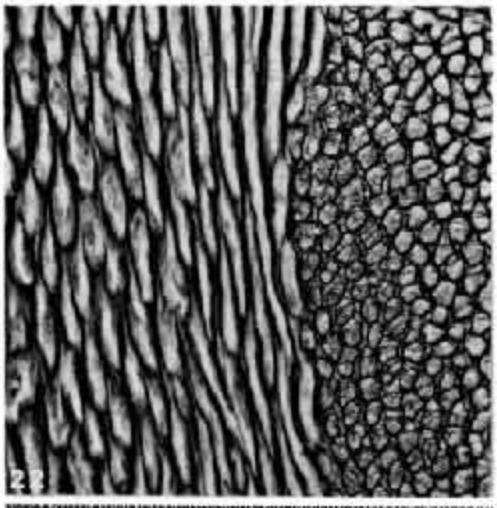
22

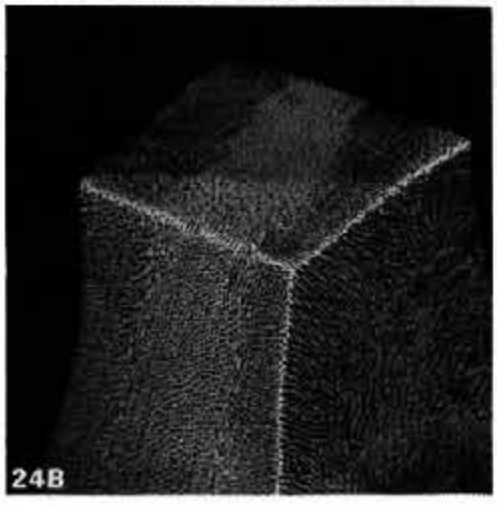
24B

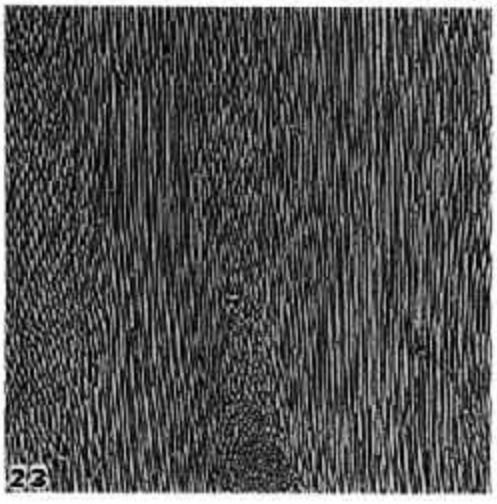
23

The present results confirm that vertical decussation does exist in rhinoceroses (Figs 1–3). We are now able to provide a more detailed description of the exact arrangement of prisms in one species, and to explain these features in terms of the developmental processes occurring in this species, the white rhinoceros, *Ceratotherium simum*. Our results also confirm Rensberger & Koenigswald's (1980) conclusion that the vertical decussation occasions the relief observed on natural wear surfaces. However, our more detailed results enable us to refine and to modify both their structural model and their hypothesis regarding relationships between structure and wear resistance.

Development and structure in Ceratotherium simum

The innermost junctional layer: the first stages

The first appearance of enamel on the surface of the mould formed by dentine is as a thin layer whose thickness is modulated by the appearance of the characteristic depressions or pits in the enamel matrix secretion caused by the secretory pole (Tomes') processes of the ameloblasts (Figs 4, 14). These pits are irregularly round and face more or less square on to the surface of the enamel. Moving a small distance occlusally on the developing surface, many pits are asymmetric, either entering the surface obliquely or showing the development of a prism boundary discontinuity with an open side—both are features from which the movement of ameloblasts and the corresponding direction of prisms deep to the formative surface can be inferred (Boyde, 1964, 1969; Figs 5, 15). The prism direction is to begin with random, but there is very soon a tendency for the majority of the pits to enter the developing enamel surface towards occlusal, i.e. the pits face towards cervical, indicating that this was the direction of translational movement of the corresponding ameloblasts (Fig. 5).

It is important to note, however, that all orientations of pits (prisms) can be found in the innermost layer. This randomness of prism orientation is best appreciated by examining the junctional region on the TSRLM. In preparations where we removed most of the dentine, we were able to demonstrate a relative 'seething' movement of adjacent prisms in this innermost layer by focusing up and down.

These same changes in orientation of prism boundaries could be seen clearly in tangential sections of the enamel dentine junction in which we prepared surfaces closely approximating the original incremental surface, by grinding and polishing (Fig. 7), air-polishing (Fig. 8), and acid etching. There appears to be a prism-boundary-free layer which is very thin before the layer in which the

---

Figures 20–23. Fig. 20. Oblique TS of white rhinoceros deciduous molar, air-polished and etched with 0.5% H_3PO_4 for 30 s showing the relative extent of the inner and outer zones of the enamel. Field width 2700 μm. Fig. 21. Higher magnification view of the same surface including the EDJ, showing that the zones of occlusal-going (Hunter–Schreger bands) and cervical-going (Hunter–Schreger interbands) do not begin immediately at the EDJ. Field width 375 μm. Fig. 22. Zone boundary in inner enamel of the same facet shown in Figs 20 & 21. Note that the prism orientation changes from the zone periphery either side of centre to the zone centre each side of the field. Field width 74 μm. Fig. 23. Same facet showing outer enamel and at bottom centre transition from inner to outer zones. Note that all the prisms are occlusally inclined in the outer zone but have a different angle with respect to longitudinal axis of the tooth so that one set of zones is cut more obliquely. Field width 375 μm. Fig. 24A,B. Stereo-pair showing the dip of a rod-shaped specimen prepared by milling away dentine and innermost enamel from white rhinoceros permanent enamel, H_3PO_4 etched. Field width 375 μm.

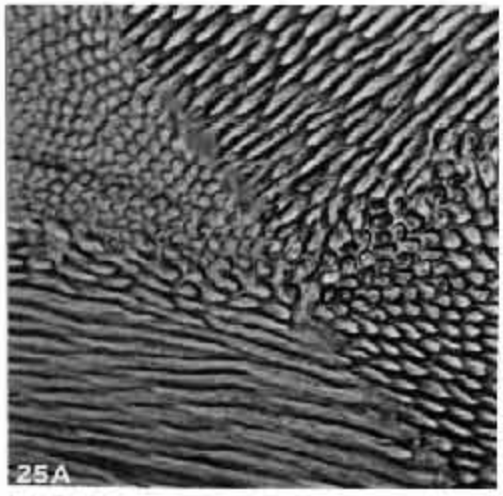
25A

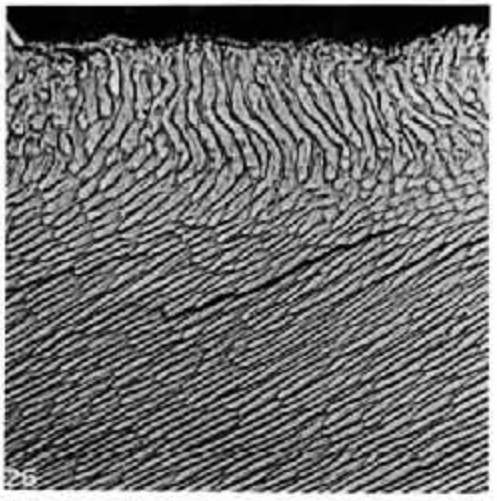
25

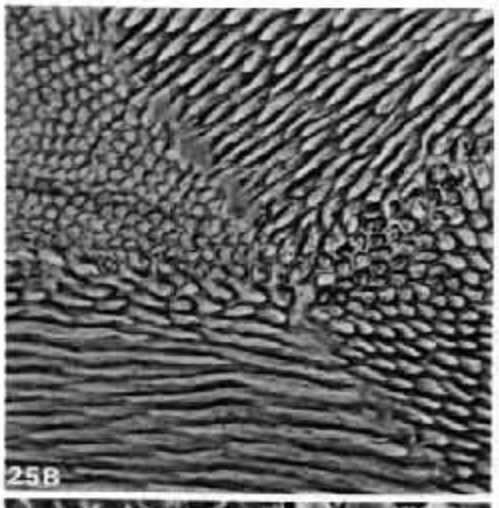
25B

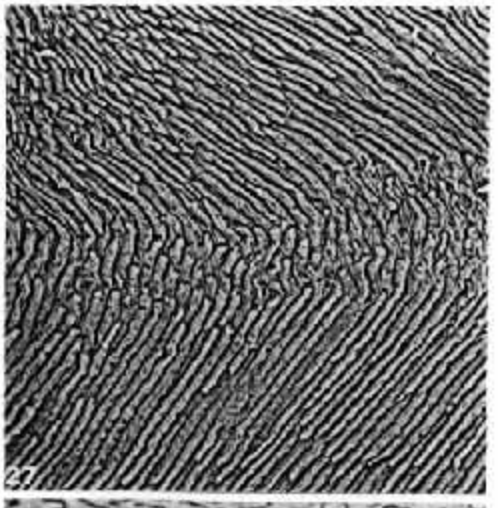
27

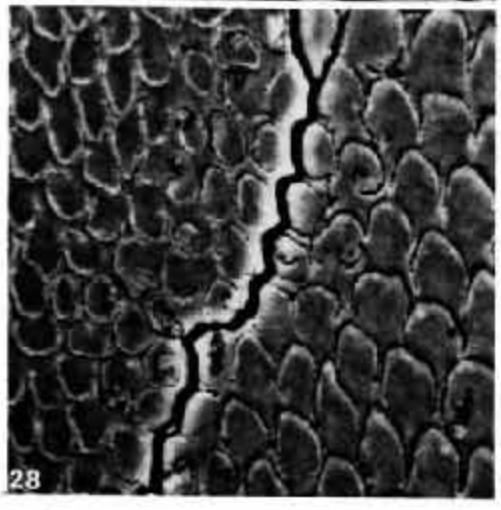
28

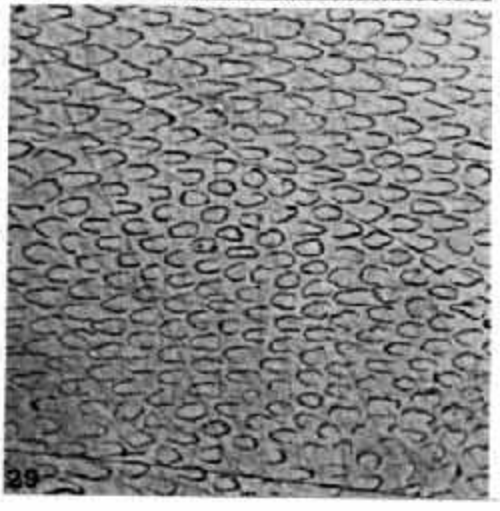
29

prism junctional discontinuities can be recognized: both this, and the succeeding layers of randomly and then predominantly cervically oriented prisms are penetrated by numbers of enamel tubules, which may obscure the interpretation of the structure in this layer. The enamel tubules can be studied in depth by LM, best by TSRLM: many are continuous with dentine tubules, but many appear to have a separate origin within enamel.

The layer of enamel next to dentine was seen to reach a much higher degree of mineralization at early stages of development than the subsequent layers, as demonstrated by the study of PMMA-embedded tissue using BSE imaging (Fig. 6). The development of the hypermineralized layer occurred synchronously with the appearance of the peritubular hypermineralized zones in the adjacent dentine.

The commencement of vertical zoning and decussation

The vertical distance along the mineralizing front (developing surface) of the enamel from the first appearance of enamel on dentine until the first obvious organization of vertical zones of pits, which enter obliquely but in opposite directions, is a few hundred micrometres. Examining the developing enamel surface proved to be a difficult way of obtaining a global view of the processes leading up to the marshalling of ameloblasts into zones: these transactions are difficult to map. It was, however, relatively easy to demonstrate a lack of order, and very easy to see the order once imposed. The first stage which clearly stands out is the appearance of narrow occlusal-going zones, which broaden out in an occlusal direction until the surface is covered with both occlusal- and cervical-going zones of roughly equal breadth. At the same time, the cervical inclination of the cervical-going prisms increases so that the contrasts due to the slopes of the pits in the contrasting zones are equal.

The impression that the occurrence of narrow zones with a steep occlusal inclination was of sudden appearance was also gained from the etched tangential sections of mature tooth structure mimicking the orientation of the developing surface. This can also be appreciated from the examination of longitudinal, transverse and oblique sections near the enamel–dentine junction (Fig. 8).

The sequence of events up to the establishment of decussation then seems to be that a more or less perpendicular orientation gives way to a predominance of cervically inclined prisms, albeit in a very thin layer. At the time that a strong occlusal movement is adopted by a proportion of the ameloblasts, an increase in the cervical movement of the remainder of the population occurs. By enrolment

---

Figures 25–29. Fig. 25A,B. Stereo-pair of 90° edge of similar small rod-shaped specimen to that shown in Figs 23 & 24. Field width 129 μm. Figs 26 & 27. Longitudinal section perpendicular to EDJ cut through a white rhinoceros permanent molar, air-polished and H_3PO_4 etched. Bulk of field in Fig. 26 is an occlusal-going zone, but note that it does not commence immediately at the EDJ. Fig. 27 shows a zone boundary between a cervical-going zone, top, and an occlusal-going zone in the lower part of the field. The zone boundary is at the centre. Field widths 200 um. Fig. 28. *Coelodonta antiquitatis* (woolly rhinoceros): portion of permanent molar enamel polished and argon ion etched to enhance prism boundary contrast. A zone boundary crosses the centre of the field. Note various round and 'coiled' prism boundaries. Field width 39 μm. Fig. 29. BSE image of surface, polished parallel to EDJ, in inner enamel of white rhinoceros permanent tooth. A zone boundary can be identified at the centre of the field with some complete, circular prism boundaries. Above and below are cervical- and occlusal-going zones with open-sided prism boundaries. Field width 82 um.

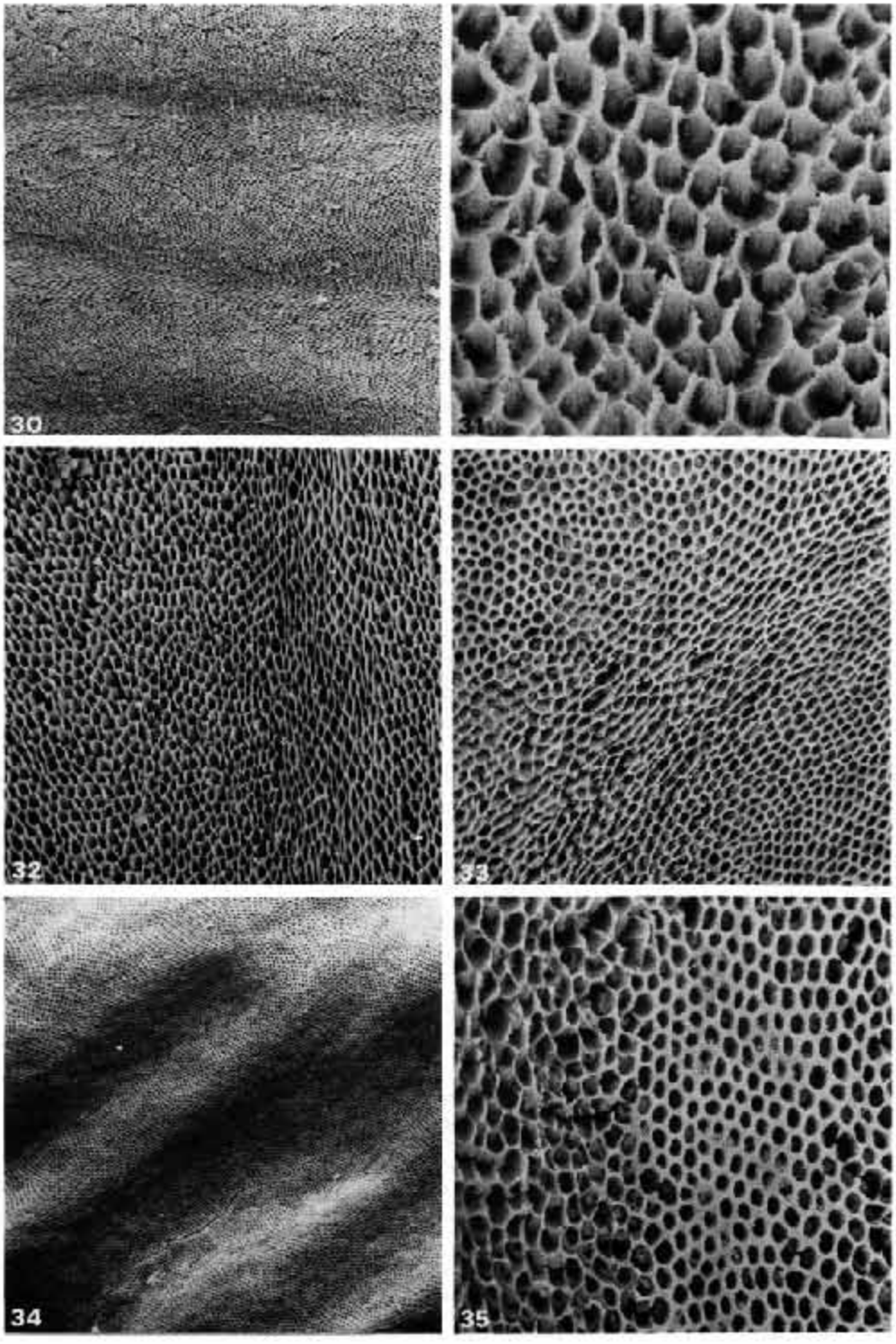
30
31
32
33
34
35

of cervical-going cells into the margins of the occlusal going zones, a balance is struck between the numbers going in opposite directions (Figs 8, 14–19).

The established inner enamel layer developmental phase

The width of the opposing zones becomes equal, and careful examination of the orientation of the steeply sloping pits by tilting and rotating the sample under observation by real-time stereoscopic SEM, showed that the slopes of the pits in the zone centres was equal for both sets of zones. This was further confirmed by the examination of the orientation of the prisms with respect to the incremental lines in longitudinal sections studied by LM (Fig. 1). The incremental line direction, of course, gives the orientation of the enamel surface at the corresponding time of the development: the direction of the prism boundaries gives the resultant direction of progress of the ameloblasts during secretion. These observations indicate that both sets of migrating ameloblasts are identical. Further evidence of their identity comes from a close examination of the zone boundaries and the other Y-junctional regions where the zones collide (Fig. 13). It is clear that prisms (ameloblasts) can move from one zone to another.

Longitudinal sections through the centres of inner-layer zones, whether studied by LM, PLM, TSRLM or SEM, show the prisms to have straight, parallel courses (Figs 26 & 27): not only is each prism parallel to its nearest neighbour, but parallel with the prisms several prisms distant. However, the SEM examination of oblique transverse sections which are cut nearly parallel with the prisms in one part of one or other set of (para)zones shows that the prisms in the other more central or more peripheral part of each parazone are cut more obliquely (Figs 21 & 22). The closer each prism is to the zone boundary the larger an angle it makes with the incremental line: this change is slight and gradual. At the zone boundary, however, the change of prism orientation increases rapidly so that there are usually some portions of some prisms to be found at the perpendicular to the incremental slope (centre of Fig. 27).

The perpendicular portions of the prisms at zone borders (Fig. 27) correlate with pits which enter the developing surface perpendicularly (Figs 11–13, 17, 19). Prisms at these locations frequently have complete, circular prism boundaries which again correlates with a zero translational velocity of the ameloblasts across the developmental surface. SEM images of the refluxed–CPD–plasma-ashed DM_3 samples mostly seem to show that these zone-border seams are proud of the surface (Figs 11 & 12), which would be in

Figures 30–35. Fig. 30. CPD, plasma-ashed surface in phase of development of outer enamel, zones running horizontally in this image. All pits are facing towards occlusal (right). BSE. Field width 462 μm. Fig. 31. Similar preparation, cervix now orientated at top of field and sample tilted so as to look nearly square into the floor of the pits, showing the true prism cross-sectional shape. Field width 43 μm. Fig. 32. Outer zone development showing a more occlusal-going zone, more obliquely oriented pits at the centre of the field flanked by two less occlusally inclined zones. Occlusal side is to top. BSE. Field width 180 μm. Fig. 33. A later stage of outer phase enamel showing a more occlusally inclined zone running obliquely across the centre of the field from upper (cervical) right to lower left. This is flanked by two valleys (the topographic contrast does not show in this BSE imaging mode) in which Pattern 1 surface zone pits can be seen. Field width 180 μm. Fig. 34. Much later stage of outer zone enamel development in which all pits are becoming Pattern 1 in morphology. Field width 473 μm. Fig. 35. Border of a groove bottom showing Pattern 1 pit morphology and the flanking enamel with a less advanced stage towards the mature enamel surface morphology. Field width 86 μm.

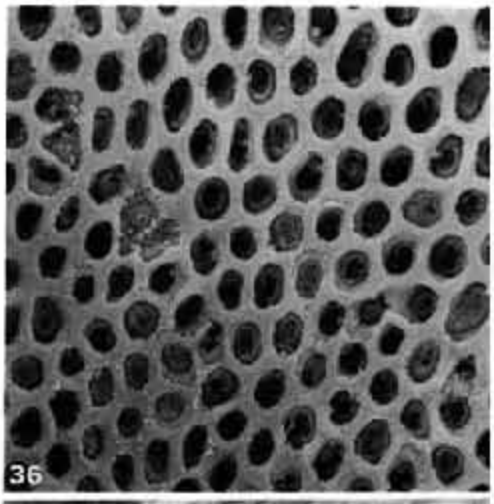
36

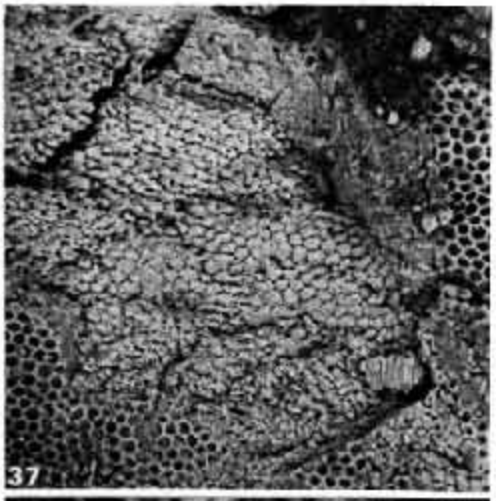
37


38

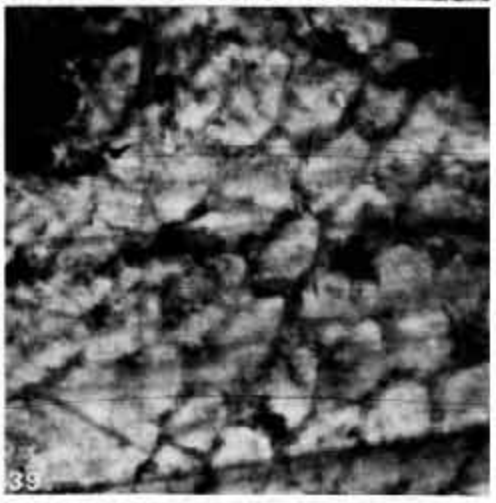
39

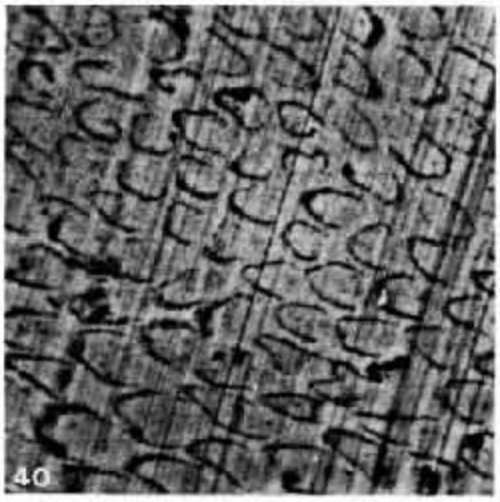
40

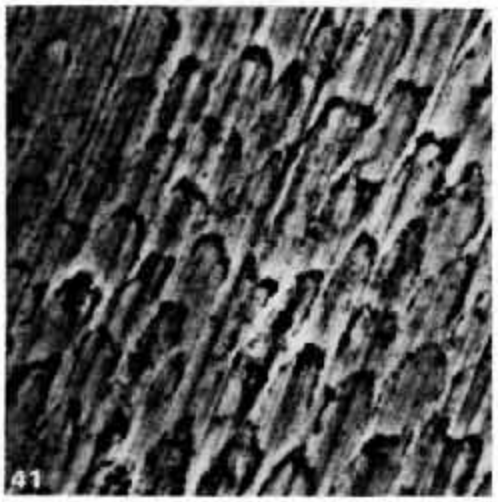
41

agreement with a local pile-up of enamel matrix happening when cells changed their direction of movement. However (apart from Y-junction nodes), transverse sections and plasma-ashed preparations (Figs 14–19) of the PMMA-embedded tissue reveal an almost smooth profile for this surface, suggesting that the zone-border ridges of inner enamel are an artefact in some way generated by the drying and shrinkage distortion of the CPD samples. That this region is peculiarly subject to preparative distortion was also shown by the NaOCl CPD samples: here the zone borders of inner enamel are always represented as valleys, indicating that the corrosion caused by hypochlorite is sufficient to demolish the delicate inter-pit wall structure of the zone borders where these are perpendicular to the surface.

SEM study of etched LSs and TSRLM study of LS cut surfaces both showed many instances where prisms change course more than once at zone boundaries in the inner enamel. Some degree of spiralling could also be recognized and this correlates with the changes in direction from one prism cross-section to the next which can be traced in surface parallel sections of the mature enamel (Figs 28, 29, 40). Such changes could be studied in detail in BSE images of polished, or polished and ion-etched enamel; the trend to spiralling and vortex or eddy formation could also be seen in TSRLM through focusing study of surface parallel sections.

The second type of interaction between the occlusal- and cervical-going zones of inner enamel occurs where these meet head-on. These collision zones are always disposed such that the narrowed end of one zone splits a broader zone of the opposite orientation (Figs 3, 10, 13). Seen at the developing surface, these Y-junctions are elevated above the surrounding surface since the colliding zone pits pile up against those of the dividing zone (Figs 9 & 13). They thus form nodes on the forming inner enamel surface which frequently have the streamlined form of the drumlins of a glaciogenic landscape.

The angles of the decussating prisms in inner enamel with respect to the incremental lines or the enamel-dentine junction were measured using the rotating stage of a polarizing microscope in LSs of mature *Ceratotherium* M_2 and DM_2 and *Diceros* M_1. In the deciduous enamel we could not reliably determine the incremental line angle as significantly different from the enamel dentine junction – indeed it was nearly the same, within a few degrees, as it is in the permanent enamel. Considering the orientations of the prisms with respect to the incremental surface, the measurements were very similar for both cervical- and occlusal-going zones.

Figures 36–41. Fig. 36. Outer zone enamel development showing Pattern 1 development with prisms within prisms and spiral or coiled prism boundaries in some of the pits. Field width 12 μm. Fig. 37 shows cementum deposition on the completed enamel surface in a white rhinoceros permanent tooth. Sharpey fibres in the cementum can be discriminated as hexagonal zones covering the same territory as the Tomes process pits in the surface of the completed enamel. Field width 200 μm. Fig. 38. SE image of natural occlusal surface of black rhinoceros molar protocone inner enamel region, showing occlusal surface ridges. SE. Field width 780 μm. Fig. 39. Part of a ridge on same natural occlusal facet, BSE imaging, showing prism boundaries, indicating that prisms in this ridge are nearly transversely interkeyed. Field width 39 μm. Fig. 40. Black rhinoceros, vector-polished section cut parallel to EDJ, occlusal face towards left, direction of polishing from top to bottom. Note prism boundaries are generally slightly wider towards the head of the prism. BSE. Field width 63 μm. Fig. 41. Black rhinoceros, vector-polished enamel sample cut parallel to EDJ. Occlusal towards top, direction of polishing from top to bottom of image. Note that prism boundaries are considerably wider at the heads of the prisms. BSE. Field width 13 μm.

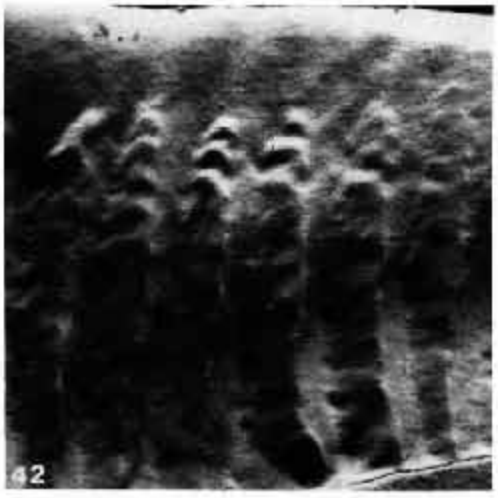
42

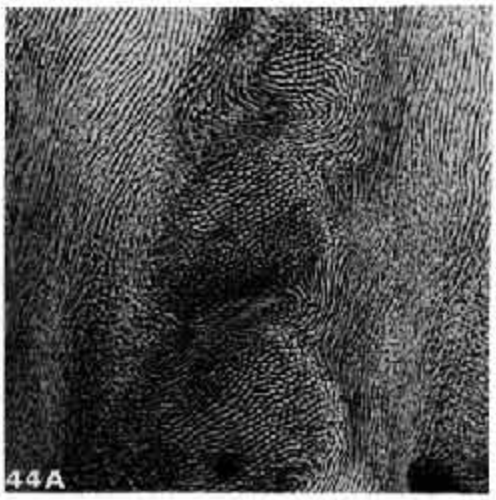
44A


43

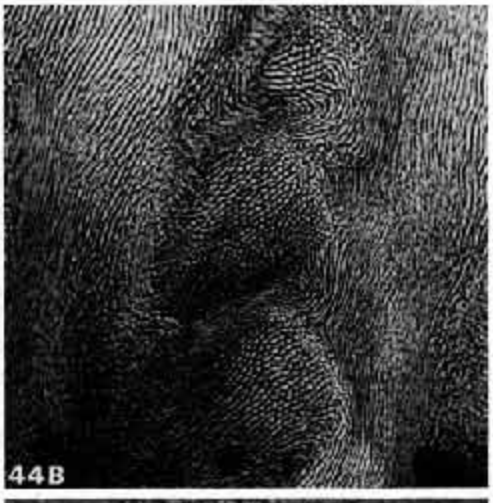
44B

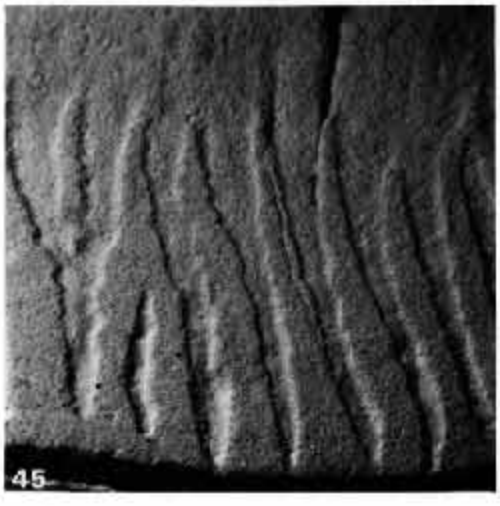
45

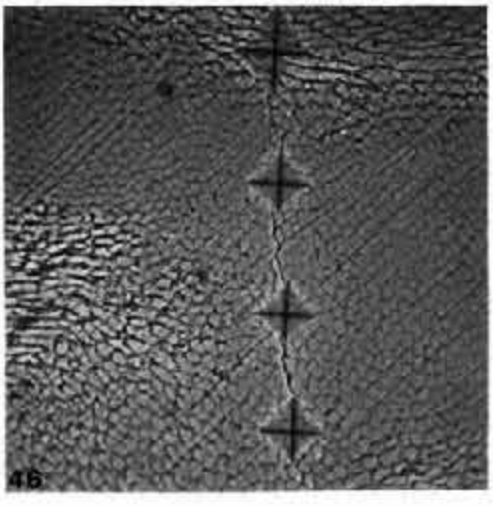
46

The outer zone

Measurements of prism orientation in LSs of the outer zone in the white rhino deciduous molar showed that all prisms inclined occlusally, but in two groups with a small angular difference of about 8° (Fig. 1). In the outermost layer, the prisms curved again to become more normal to the surface.

In the white rhinoceros permanent molar outer enamel, the angle between the occlusally inclined prisms and the incremental lines was 58.5° and 43.5° for two major groups: i.e. 31.5° and 46.5° to the surface normal. Again, the inclination changed to more normal on the outermost layer, being in the range 4–17°, mean 12°, to the surface normal.

These measurements show that the transition of the occlusal-going prisms from the inner to the outer layers, which can be seen in LM, TSRLM and SEM to be a gradual curve, involves a change in course of about 30°. The same, now more occlusal-going, prisms undergo a further bend of 14.5° to reach the surface at 17°. The cervical-going prisms of the inner layer bend through a much larger angle to assume an occlusal-going orientation—though less occlusal-going than their opponents in the outer layer. They also undergo a change of orientation in the outermost to proceed more normal to the surface.

Summarizing the observations of prism angles as seen in LS we find that there is also a vertical decussation of prisms in the outer layer (and to a limited extent, even in the outermost layer), but this decussation is between two sets of prisms in different zones which both incline occlusally, but to a different extent: the contained angle between the prisms in contrasting zones, as seen from the tooth surface, reduced from a measured maximum of 122° in the inner layer, to 15° in the outer layer of permanent enamel, and even less, about 8°, in deciduous enamel. The differences in the angle of entry of the pits at the developing surface which correlate with this arrangement can easily be seen in views of the surface at magnifications of 2000× in the SEM, but since this corresponds to a field of view of only 50 μm wide, it is not easy to study the pattern of decussation at the developing surface during outer layer formation.

The best confirmation of the existence and the extent of the decussation of prisms in outer layer enamel comes from SEM study of etched (Fig. 23) oblique TSs and air-polished TSs (Fig. 49), which cut both sets of zones of prisms obliquely, but one more obliquely than the other (Fig. 23). This method independently confirms the observation that the decussation angle in outer enamel is greater in permanent than in deciduous teeth.

The transition between inner layer and outer layer formation as seen at the developing surface could be traced in the SEM, since the larger deciduous

---

Figures 42–46. Figs 42, 43, 44A,B. Same region of black rhinoceros, oblique LS, airbraded with 10 μm alumina in SS White Industrial Airbrasive Unit, H_3PO_4 etched to reveal prism orientation. Fig. 42, field width 1800 μm, CBSE view extending from EDJ to enamel surface to show the region from which the succeeding three pictures were taken. Fig. 43, field width 410 μm, CBSE. The undulations on the diazole ridges show that there was a regular variation in the course of the prisms. This is a severely 'airbrasion' etched specimen, in which the magnitude of the change in prism course corresponding to these undulations has been exaggerated. Fig. 44, stereo-pair BSE, field width 360 μm. Fig. 45. Oblique TS of white rhinoceros permanent molar cut parallel with prisms in occlusal-going zones, lightly airbraded. Unidirectional BSE. Field width 1800 μm. Fig. 46. Diamond-polished section of black rhinoceros permanent molar enamel, showing part of a row of microhardness indentation marks. These were found to be largest in more longitudinally intersected zones. BSE. Field width 180 μm.

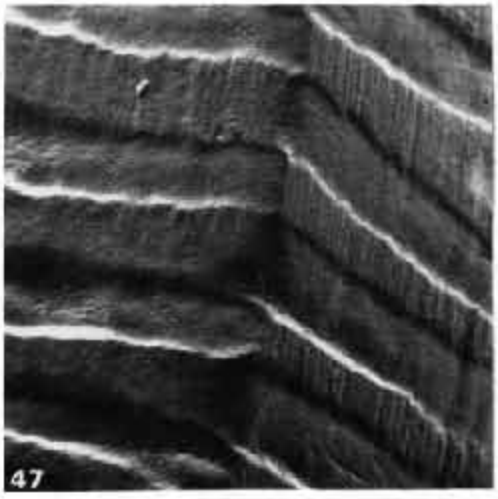
47


48

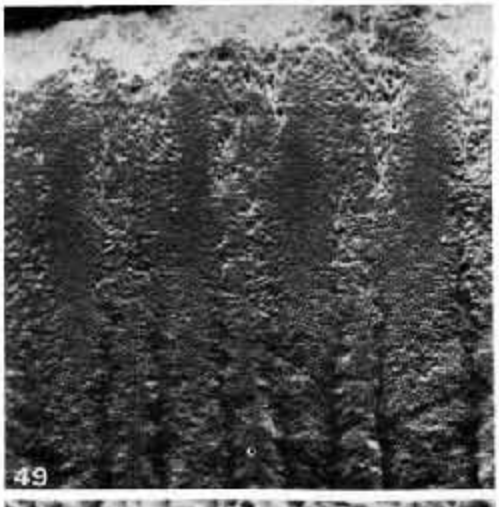
49

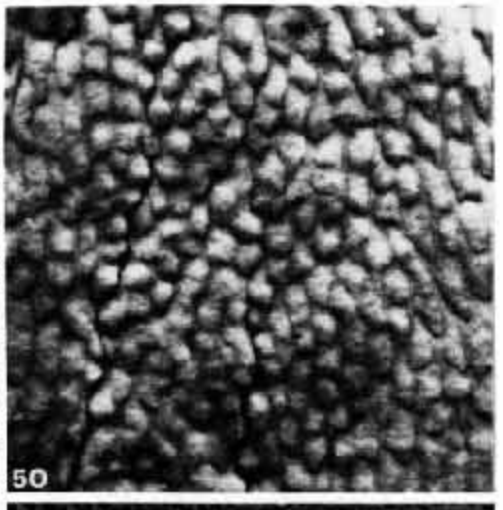
50

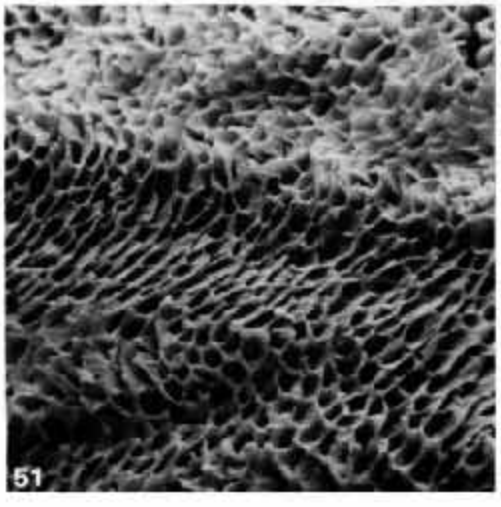
51

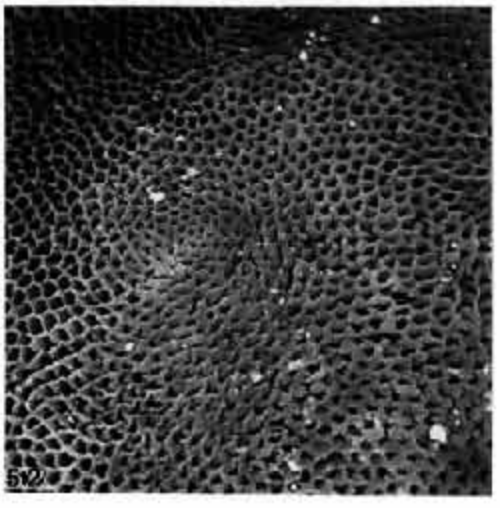
52

molars which we studied showed every stage of enamel development from the coverage of new dentine to the completion of the mature surface morphology in single specimens. The transition is associated with an increasing proportion of pits entering from (i.e. facing) occlusal (compare Figs 9–19 with Figs 30–35). The last portions of the still recognizably cervical-going zones are narrow, tapering towards occlusal and reminiscent of the similarly narrow first cervical traces of the occlusal-going zones. The borders of these last cervical-going patches are not sharply defined: they are surrounded by bands of a few pits undergoing a series of changes in orientation from occlusal-going, through oblique transverse and transverse-going directions. These intermediate orientations explain the wavy (transverse) component of some of the prism courses which can be discerned in transverse sections in the LM at the inner outer layer transition. The transition zone could be located in low-magnification SEM views of the CPD and CPD–plasma-ashed material from the disappearance of a regular herringbone cracking pattern which appears in the zone borders of the inner layer, which occurs with this preparation method.

Examination of the gold-coated, CPD, plasma-ashed 'SEM' specimens using a stereobinocular microscope and reflected light (Fig. 3) provides direct confirmation of the continuity of the zones of the inner and outer layers. If the direction of illumination is oblique from cervical, the zones appear with high contrast and with uninterrupted continuity across the transition region. If the light is directed obliquely and from the side, however, it is easy to follow the increasing amplitude of the ridges which the zones manifest in the developing outer layer: this can also be studied with high topographic contrast imaging modes in the SEM, such as the CBSE and BSE-ET methods used here. The occlusal-going zones in the inner layer, whose pits (and prisms) become less steeply inclined but are still more occlusally inclined than the contrasting zones, develop into progressively more prominent ridges in the outer layer. Conversely, the originally cervical-going zones of the inner layer, which become just occlusal-going in the outer layer, become deeper valleys in the outer layer.

Thus, SEM images of early outer layer development show relatively flat surfaces (e.g. Fig. 30) in which zones of more and less inclined pits can be recognized (Figs 31–33). Progressing through the development of the outer layer, these zones change so that there is a contrast between obviously inclined pits in the ridges and more symmetrical pits facing more perpendicular to the surface in the valleys (Figs 34 & 35). Looking at the frequency of artefactual

---

Figures 47–52. Figs 47 (CBSE), 48 (BSE). Black rhinoceros specimen cut with two 45° TS faces intercepting each other in the inner enamel. Air-polished, showing the removal of the cutting scratches in parazones, and how the parazones of one face become the diazones of the opposite face of the other face, and vice versa. Field widths 790 and 900 μm. Fig. 49. Black rhinoceros TS, air-polished, outer zone showing that the zone boundaries of the outer portion of the inner layer which is seen at the lower part of the field have retired deeper than the occlusal- and cervical-going zones. In the outer layer, the upper half of the picture, little etching has occurred, since there are minimal changes in prism orientation in this region. SE. Field width 680 μm. Fig. 50. Region of transversely intercepted prisms in black rhinoceros air-polished sample, showing peculiar etching at zone boundaries so that prism cores project as mounds from the surface. BSE. Field width 90 μm. Fig. 51. CPD, plasma-ashed preparation of developing enamel surface of a small loph tip from a lower deciduous molar of a camel fetus showing horizontal (side to side) orientation of decussating zones. SE. Field width 180 μm. Fig. 52. Developing enamel surface in tooth lower first permanent molar tooth germ showing tip of small cusp. Note spiral pattern to be seen in direction of Tomes process pits. SE. Field width 158 μm.

cracking in the CPD, plasma-ashed samples, a rough crazing developed more often in the ridges, suggesting that either they may be composed of a less mature enamel (which because it contains more water, shrinks more and cracks more), and/or that the structure is more discontinuous. The former idea would correlate with the fact that the more occlusal-going zones (the ridges) at any one level are younger. The latter idea fits with the fact of an increasing proportion of Pattern 1 prisms in the more mature enamel represented by the groove bottoms. Pattern 1 prisms form in pits which have a floor separated from the inter-pit walls: they therefore have separate, circular prism boundaries. As immature enamel shrinks, Pattern 1 prism cores shrink onto themselves leaving the separate and continuous inter-pit, 'interprismatic' phase to remain intact, perhaps shrinking as is fit to its water content. Pattern 3 prisms, and the majority of prisms throughout inner layer and outer layer development in *Ceratotherium* are Pattern 3 (though with obvious local patches of Pattern 2 arrangement), have open sided boundaries due to the continuity of pit floors and walls at these sites: as immature enamel shrinks, therefore, the prism boundary cracks extend to split through into the neighbouring boundaries, thus cracking up the enamel.

The amplitude of the ridges in the developing outer zone was possibly also increased by preparative distortion of the CPD samples, so this was checked using transverse sections of methacrylate-embedded DM_3, and by studying the incremental line amplitude in TSs of permanent teeth. Both gave values in the range 20–40 μm, for all but the outermost layer of the enamel. Direct examination of the completed-thickness enamel of nearly mature DM_3 lophs, unerupted mature permanent teeth, and the study of TS of mature teeth show that the ridge amplitude may exceed these values in outermost enamel. Through-focusing measurements with the TSM gave values of about 75 μm. Thicker, late ridges are also thicker because incremental growth continues for a little longer on ridge crests. Thus it was possible to see some incremental layers on ridges overlapping onto the valley enamel in TSs. This continued growth over ridges would mean an increased time interval between the secretory phase lifespan of the ridge (ex inner layer occlusal-going) and valley (ex inner layer cervical-going ameloblasts).

The continued growth on ridges inferred from the incremental line pattern accords with the developmental surface picture seen by SEM that we have just described, where clearly active secretory phase pits are seen on ridges next to valley bottom pits which do not change their morphology in tracing the valley further occlusally, indicating that these ameloblasts have stopped producing enamel – that this surface has stopped growing.

The enamel surface and outermost layer

Following the CPD, plasma-ashed DM_3 developing tooth samples even further occlusally led to an ever increasing number of the ameloblastic pits showing the Pattern 1 morphology—a continuous inter-pit phase separated from symmetrical pits with separate boundaries. The transitions here described occur first in the valleys, and later on the ridges. These pits do not completely fill in with enamel. Instead, a ring or rim of enamel forms a partial floor just inside the pit wall (the main prism boundary: Figs 35, 36). Some of the pits have flat floors, but the floors are always deep. Thus the completed enamel

surface has a pitted morphology which is so prominent that it can even be seen in low-magnification LM images of obliquely sectioned surface enamel.

It is not possible to provide a more accurate description of prism courses in the outermost layer because of the interaction of the ridged surface morphology giving rise to local changes in orientation of the surface. However, the prisms often seem to be within 5° of the local surface normal. The inner part of this outermost layer also contains some very prominent isolated prism boundaries appearing dark in transmitted light and very bright in the TSRLM. Some similarly prominent boundaries occur in the innermost layer.

Cement deposition

Cement deposition was examined in one mature white rhinoceros M_3 protoloph on the internal aspect. Areas with thin cement show a hexagonal pattern with hexagons exactly matching the areal distribution of the underlying enamel pits (Fig. 37). The strong suggestion that these areas are mineralized Sharpey fibres of cementum may be countered by the proposal that an otherwise uniform layer of cement might craze due to shrinkage. Since the cement would be thinner over the inter-pit walls, it would fail at these locations on drying.

TSRLM study of the thicker bands of cementum, which grows as a series of mainly transverse, but branching continuum of bars or beams, showed that it was cellular, with a remarkably symmetrical radial distribution of the canaliculi of the cementocyte lacunae. An unusual form of branching canals was seen in this cementum, which should be the object of future study.

Wear

We examined several different mechanisms which result in the loss of enamel tissue, and paid particular attention to the relationship of oriented structures (crystals, crystal groups, prisms and zones in the sense of Hunter–Schreger bands) to the rate of removal of the tissue. Natural wear (Figs 38, 39); attempts to produce flat, polished surfaces by polishing against diamond laps (Figs 29, 40, 41, 46); airbrasion with an air-propelled stream of alumina particles (Figs 42–45); air-polishing with an air-propelled, water-shrouded stream of sodium bicarbonate particles (Figs 47–50); microhardness indentation (Fig. 46); and ion beam erosion (Fig. 28) all showed differential rates of removal which could be related to structure orientation. In the previous section we have described the structural organization and how it relates to the development of the tissue. Here we see how the structure relates to wear properties.

Natural wear facets

Natural wear facets, as studied directly by stereobinocular light microscopy, reflected light microscopy of transparent casts of silicone rubber replicas and direct examination in the SEM, all showed the presence of grooves and ridges on occlusal facets which matched the size range and distribution of the Hunter–Schreger band zoning. By the examination of the wear facets directly in the SEM and using BSE density-dependent imaging, it was possible to demonstrate that ridges on the wear surfaces correlated with regions where the prisms approached the worn surface more normally; conversely, grooves

correlated with areas where the prisms were more nearly parallel with the worn surface (Figs 38, 39).

Rensberger & Koenigswald (1980) described two types of ridge developing on occlusal surfaces: B ridges, which they considered to be in the inner part of the inner layer enamel, and A ridges, which they considered to be in the outer part of the inner layer enamel. We have been able to find these ridges, but conclude that the A ridge type is in fact located in the outer layer enamel. Rensberger & Koenigswald (1980) concluded that the prisms in the outer layer enamel were parallel, although they were ambivalent about the exact orientation of the prisms in the outer layer. We show here that the prisms in the outer layer still continue to decussate even though both sets of zones are occlusally oriented.

The orientation of the outer part of the worn occlusal surface is such that the two zones of occlusally oriented prisms will intercept the surface differently. The more occlusally oriented zones of the outer layer, corresponding to the original occlusally oriented zones of the inner layer, are more perpendicular to the surface. The less occlusally inclined zones, corresponding in the inner layer to the cervically inclined zones, have a component which is more parallel with the occlusal surface, and will therefore be worn more rapidly. The fact that the decussation angle between the prisms in the inner layer is greater than those in the outer layer explains the greater relief of the ridges in the inner layer. It should be made clear that in tracing a line from the enamel dentine junction to the natural enamel surface across a worn occlusal surface, if one intercepts a ridge in the inner enamel and traces to the surface, this corresponds to a valley in the A ridge zone in the outer enamel. Likewise, valleys in the B ridge zone of the inner enamel correspond to the shallow ridges of the A ridge zone in the outer enamel. This explanation of the occlusal surface ridges is considerably simpler than that given by Rensberger & Koenigswald (1980) and corresponds with the known orientation of the prisms.

Polished surfaces including vector polishing

Our first reason for using diamond polishing techniques was to produce very flat surfaces, which we hoped would be free of topography and which we could therefore use to produce density-dependent images using BSE detection. We were partly thwarted in this aim by the fact that it is difficult to polish rhinoceros enamel flat due to the variations in hardness (abrasion resistance) associated with structure orientation. However, such BSE images were useful in interpreting exact details of prism cross-sectional morphology at different levels through the enamel.

In order to understand the relationship of polishing wear to orientation, we mounted small blocks of enamel which had been cut in specific orientations with respect to the structure on one large specimen stub with their orientations clearly defined. This large specimen was ground and polished to one level, keeping the polishing direction in the final phases of polishing well oriented, so that we knew the direction of progression of the diamond polishing surface past the surface of the specimen. Thus on the same specimen we could compare the abrasion caused by a side-to-side movement across transversely sectioned prisms compared to the tail-to-head or head-to-tail movement, likewise we could compare the effects of prisms lying transversely, obliquely or nearly longitudinally in the surface (Figs 40 & 41).

Again, it was found that regions in which the prisms met the surface more perpendicularly were selectively resistant to polishing abrasion, and a low-amplitude surface relief developed with the valleys corresponding with areas where the prisms were more parallel with the surface. At a higher resolution it was possible to discriminate differences in the fine texture near prism boundaries which we could relate to the orientation of the enamel crystallites in the prism boundary region with respect to the 'abrasive vector' (in our sense) of the polishing process.

In obliquely sectioned zones, the top of the 'horseshoe' or 'arrowhead' of the prism boundary was always more 'torn out' by the soft-lap diamond polishing (Fig. 41), resulting in a widening of the apparent prism boundary at this location: more material was lost from the prism head side of the boundary, i.e. from inside the prism. In transversely sectioned prisms, more material was lost from the 'tail side of the next prism', i.e. from the material of inter-pit origin (Boyde, 1964), next to the prism boundary. Both these findings suggest that groups of crystallites (using the sense of enamel crystal groups as crystal clusters with parallel a and c axes as described by Ronnholm (1962) and Boyde (1964)) tend to break away from the polished surface more when (a) they have a larger component of orientation parallel to that surface, and (b) there is some nearby room or space for bending (and thereafter breaking) to occur, owing to the proximity of the enamel prism boundary or crack. Polishing damage near the prism boundary head was greatest when the polishing vector was in the head-to-tail direction (Fig. 41) rather than in the side-to-side direction (Fig. 40).

Airbrasion

Airbrasion using alumina airbrasives in the SS White industrial airbrasive unit to erode oriented sections of rhinoceros enamel produced rapid and dramatic effects, as described by Rensberger & Koenigswald (1980). The simplest surface to understand was that of the 45° TS cut so as to mimic the orientation of an occlusal surface (Figs 42–45). Such surfaces eroded very rapidly in the region of the zones with prisms parallel to the surface. The rate of erosion in more peripheral enamel for a given crude dose of airbrasion (this process is difficult to quantitate) was less than in the inner enamel. In black rhinoceros enamel, peculiar undulations of the surface of the parazones in the more peripheral inner layer of enamel were observed (Figs 42–44). These correlated with a less straight course of the prisms that could be observed using polarized light microscopy on oblique transverse sections, again showing that even fairly small changes in prism course can make a very important difference to the rate of airbrasion.

It should be noted that the airbrasion process itself leaves a crudely pocked surface in which the impressions of the individual cutting particles can be discerned. Thus, in order to determine prism orientation we had had to use a light phosphoric acid etching to bring out the prism structure (e.g. Fig. 44). Since the surface relief was so great as a result of the airbrasion process we felt that the phosphoric acid etching, which would not have been likely to remove more than 1–2 μm enamel, would not contribute to the total relief.

Air-polishing

We used the Dentsply Cavitron air-polishing unit and discovered that this caused differential erosion of the enamel, again with a much greater removal of

tissue in regions where prisms lay more parallel with the surface (Figs 47–50). Further, the enamel dentine junction region seemed to be more resistant to erosion, and the more peripheral regions of the enamel, particularly the outermost region, were less abraded than the inner zones.

Prism shape and orientation can be discerned in an air-polished surface without resorting to the use of etching, since this process itself etches out the prisms with the more peripheral regions of the prisms close to the prism junctions being removed more rapidly (Fig. 50).

Air-polishing removes dentine and cement so much more rapidly than enamel that it was possible to prepare surfaces which must have been a close approximation to the real surface of the enamel, although covered with cement, and of the enamel dentine junction, merely by air-polishing these surfaces.

Microhardness testing

Microhardness indentation testing showed that diazones in 45° TSs showed a greater hardness than parazones (Fig. 16).

Ion beam etching

Ion beam etching is a process in which individual atoms may be removed as a result of collision sequences initiated by a bombarding atom beam, whether those atoms are ionized or not. Ion beam erosion can be a conservative etching procedure to bring out the details of prism distribution on a polished surface if used with sufficient caution. Thus, it is possible to control the total amount of tissue removed to the micrometre level. We noted that there was a superficial resemblance between the low, mounded appearance of roughly transversely intercepted prisms in ion-beam-eroded surfaces (Fig. 28), and those produced by the air-polishing process (Fig. 50). This result suggests that the possibilities for loss of material in both cases may be greater at prism boundaries.

DISCUSSION

Vertical decussation

All our findings support the existence of a vertical prism decussation in the inner one-half to five-sixths of the enamel in all the rhinoceros species examined. This decussation begins very close to the EDJ. Despite a unity of basic structure, there are characteristic differences in detail between species. Since developing enamel was available only for *Ceratotherium simum* we chose to investigate the development and structure of the enamel in that species in detail.

The developing enamel preparations examined in the SEM clearly showed that prism decussation does not begin immediately at the EDJ. To begin with, the prisms leave the EDJ perpendicularly though with individual prisms describing considerable variations from this course. Only after this layer of enamel has been formed do they assume an average course which is lightly cervically inclined, again with individual prisms and groups of prisms deviating from this course. When this very thin layer of enamel has been formed, vertical decussation as such commences, and it is possible to find large fields of prisms which are coursing either occlusally or cervically. The occlusal-going zones are

to begin with in the minority, but a balance between numbers of occlusal- and cervical-going prisms is soon reached. It is particularly important to notice that we find no trace of organized groups of prisms coursing in a lateral or horizontal direction, as is the case in the horizontal decussation in other extant mammals (e.g. Figs 51 & 52). Examination of a very small (white rhinoceros fetal) cusp centre which had grown to dimensions of approximately 1 × 2 mm showed that the vertical decussation had commenced in this small structure.

In a similar cusp centre of tapir we found that the zones of decussating pits were concentrically arranged with respect to the cusp tip, much as in Kawai's (1955) figure of the adult structure of ursid enamel (Fig. 52). This throws some doubt on the suggestion of Rensberger & Koenigswald (1980) that vertical decussation arose phylogenetically through a modification of the basically horizontal decussation seen in certain lophodont mammals such as tapirs, in which the horizontal pattern is tilted towards occlusal between lophs. The basic difference appears to be that the decussating zones are always parallel with the formative differentiating edge of the enamel in the case of horizontal decussation, and this is true even if the formative edge resumes a strongly curved shape, as is the case in both the tapir and camel which we investigated in this study.

One 'artefact' of sectioning the inner layer, decussating enamel needs to be discussed in terms of the possibility of prisms crossing from one zone to the next, or of their moving transversely across the long axis of the tooth to any significant extent. A really true TS with respect to the tooth axes cuts the zone structure slightly obliquely. In such sections the prisms in adjacent zones appear to incline towards each other. The greater the obliquity of the TS (up to 45° to the longitudinal), the greater the appearance of the prisms inclining across the axis of the zone to which they belong. If a transverse section is also oblique in the sense of not crossing the zones perpendicularly, then it appears that the component of prism orientation resolved in the plane of section differs in the two sets of zones. In fact, it is possible to generate sections with longitudinally cut zones with prisms parallel with them, and the alternating zones with prisms crossing them at right-angles. All these possibilities are simple consequences of the packing pattern, for which we satisfied ourselves by a simple plasticine model building and sectioning experiment.

One interesting correlate of the total cell movement prism course described during the development of rhinoceros enamel is that cells associated with cervical-going zones finish at the completed surface of the enamel at a different developmental level than those which move occlusally. In mammals in which little decussation or horizontal decussation occurs, cells leaving the enamel dentine junction at one developmental stage finish up at the completed enamel surface closely placed with respect to one another in terms of their developmental horizons. However, in the rhinoceros, the cells suffer a considerable vertical stratification and we can deduce that those which move cervically not only finish further towards the cervix but have also been functioning for a longer time when they reach the surface of the tooth. This conclusion is substantiated by the observation that the stages of maturation of the enamel surface are reached earlier in the grooves of the completed enamel surface which represent mainly the sites of cells which had belonged to cervical-going zones in the first place. This has considerable theoretical interest.

As regards the analysis of cell movement patterns in the plane of the developing enamel surface (rather than their three-dimensional course) we can analogize the movement of the vast hordes of ameloblasts concerned with making these large surface areas of enamel with either the dancers on an infinite dance floor, or soldiers participating in an immense ceremonial parade. In both cases large columns of moving objects standing essentially perpendicular to a surface are moving past one another, interacting with each other at zone boundaries. It can therefore be no surprise that ameloblasts (prisms) at zone borders seem to describe eddy vortices which possibly result from buffeting due to attempts of neighbours to move in opposite directions simultaneously. We believe that it is possible that prisms occasionally move round each other, meaning that ameloblasts did the same during formation at zone boundaries.

The analogy with a ceremonial parade also has its uses in considering what happens at Y-junctions in the zone pattern in inner enamel. Where one column or zone of ameloblasts is advancing into a wider zone progressing in the opposite direction, the cells pile up on top of each other as the ones in the front rows are being pushed by those behind. The result in terms of developing surface morphology is that the portion of surface under these cells rises to a mound, presumably because the obstruction causes them to move less across the surface. These mounds are what we have described as nodes or drumlins in the foregoing.

Wear

The present results suggest that the processes of real occlusal wear during tooth function can be compared with the procedures of polishing, air-polishing and airbrasion which we have used in specimen preparation. They all seem to be closely related in terms of enamel tissue loss mechanisms. In each case we find that units of enamel structure which are parallel with a surface under wear are lost more rapidly than those units which project perpendicular to the enamel surface.

Natural occlusal facets showed nothing which would suggest that whole prisms were dislodged from the surface (Figs 38, 39). We suggest, therefore, that the amount of tissue removed in natural attrition and abrasion events is seldom either a whole prism or a flake containing many prisms. It is, rather, a fragment of a prism.

Considering the ultrastructural organization of prisms we could examine the possibility of two sub-prism dimension units as features which might influence the fracture of this tissue by natural wear. These are the apatite crystallites themselves, or the parallel groups of crystallites. It is an aspect of enamel ultrastructure which can best be understood from TEM studies of early, immature enamel and which is almost universally overlooked, that the flattened hexagonal cross-section crystallites are stacked as c-axis parallel groups with their flat sides also parallel. The crystallites within a group are exactly parallel, but adjacent groups may be only nearly parallel. There exists the possibility, therefore, that rupture of enamel may occur preferentially between groups. These are substantially greater portions of the prism cross-section than the crystallites of which they are composed. Only future studies could determine whether there is some sounder basis for this particular speculation.

We suggest that this applies to enamel structure at several different levels, possibly at the level of the unit crystallite, almost certainly at the level of parallel groups of crystallites, and certainly at the level of individual prisms. In the natural case we feel that it is more probable that enamel is lost as small groups of crystallites simultaneously. In the artificial air-polishing and airbrasion cases it is possible that whole lengths of prisms parallel with the surface may be lost at any one time. The correlations that we find between these different methods of wearing enamel make us able to suggest that vertical decussation has a real functional advantage, as proposed by Rensberger & Koenigswald (1980). These authors have proposed that vertical decussation confers a greater resistance to wear, but they did not offer a mechanism.

We draw attention to three aspects of the organization of rhinoceros enamel which would tend to increase wear resistance. In the first place it is obvious that the decussating zones themselves are not parallel to the wear surface, whereas in a tooth with horizontal decussation whole sheets or prisms may be parallel with the occlusal surface and occasionally cleave away as units. In the second place the well-oriented vertical decussation in the rhinoceros means that the prisms do not present the oblique direction which can be described through Pattern 3 enamel at the wear surface. An analysis of fracture mechanisms in Pattern 3 enamel was given by Boyde (1976). This indicated that this type of enamel is weak in response to forces which tend to cleave it so as to join up neighbouring prism boundaries where the end of the open side of the horseshoe-shaped boundary is at its closest to the closed side of its nearest neighbour. In this case it is only necessary to separate adjacent parallel crystallites from one another. Attempts to cleave enamel in a direction exactly parallel with the rows which can be traced through Pattern 3 enamel means that crystallites in the narrow tail portions of the prisms have to be ruptured under tension: this type of cleavage is therefore more difficult to induce. Rhinoceros enamel prisms lie in this position. Thirdly – and this is possibly the most important point – vertical decussation would tend to prevent cleavage of overhanging or unsupported prisms which would otherwise occur in association with the high occlusal relief which develops in rhinoceroses.

It is a well recognized fact in human clinical dentistry that enamel will cleave parallel with the prism direction if the prisms do not radiate back on to sound dentine. It is probably always the case that decussation, whether vertical or horizontal, is designed to minimize the incidence of massive cleavage through enamel. Only vertical decussation can prevent this happening under normal functional circumstances.

Our analysis of the natural wear surfaces of rhinoceros enamel and the development of the A and B type ridges as described by Rensberger & Koenigswald (1980) shows that both relate to vertical decussation. The two types of ridge have a different relief because of the different nature of the vertical decussation in the inner and outer layers. The functional advantage of the development of a microrelief on biting surfaces is questionable, but it might well be that rough browse is better comminuted by serrated than by smooth cutting edges. Compared with tapirs, rhinos are distinctly more hypsodont, and it is at least a plausible hypothesis that the diet of the first rhinoceroses was tougher than that of the probably ancestral tapirs. It is equally likely, however, that the functional advantage, if such there be, of enamel with vertical

decussation is not to give rise to this relief, which is an accidental consequence of the vertical decussation, but that it is important in allowing for a higher macroscopic occlusal relief by preventing the enamel from cleaving away when the supporting dentine has been removed.

We are able to point to clear species differences between the organization of the inner enamel, i.e. that showing vertical decussation, in the two recent rhinoceros species which we have examined. Simplifying, the white rhinoceros shows relatively straight uncomplicated zone boundaries, with the prisms within the occlusal- and cervical-going zones running straight courses. The zone boundaries in the black rhinoceros enamel are more convoluted, and the course of the prisms within the zones is more sinuous, suggesting perhaps a greater exchange of prisms between zones at zone boundaries, but in any event a greater mechanical interlocking of the zones. In this respect it is interesting to note that occlusal relief in the black rhinoceros is considerably greater than in the white rhinoceros, again suggesting the importance of the prevention of massive cleavage as a functional advantage of the adaptations which we are considering. In the case of extreme overhanging or unsupported enamel, it might be the tendency for cleavage at zone boundaries which would limit the strength of the tissue. This tendency is reduced by interlocking at zone boundaries. Since it is almost certain that the white rhinoceros is descended from the black rhinoceros (Hooijer & Patterson, 1972), the simple structure is likely to be derived, and we predict that the more complicated structure is what will usually be found in rhinoceroses which do not have the modified occlusal morphology with low relief of the white rhinoceros. The modified low relief in the white rhinoceros is associated with a grazing specialization as opposed to the ancestral browsing condition characteristic of rhinoceroses in general (Osborn, 1903; Fortelius, 1982).

We note in passing that our results clearly show that enamel structure influences microwear patterns, and that reconstructions of the diets of extinct species based on microwear analysis must therefore take this further complication into account, as already emphasized by Rensberger (1983) and Fortelius (1984). It is conceivable that foods with different wear properties may bring out the relief due to enamel structure in different ways, and, conversely, that similar foods may result in different wear patterns depending on the structure of the enamel.

Not the least interesting aspect of the development of rhinoceros enamel concerns the elegant cell movement patterns which the ameloblasts describe. At present we are unable to indicate the nature of the forces and controlling mechanisms which cause these cells to move as they do. These must be the objects of future study. We only hope that the fundamental mechanisms could be worked out on other species which are not in such an endangered situation from the conservation viewpoint.

ACKNOWLEDGEMENTS

This study has been supported by an exchange grant between the Royal Society and The Academy of Finland to M.F. and by Medical Research Council and University of London Central Research Fund grants to A.B. We thank Stephen A. Reid for help with the microhardness testing, and Elaine

Maconnachie and Roy Radcliffe for skilled technical assistance. The mature specimens were loaned by the British Museum (Natural History) through the kind auspices of Dr Juliet Jewell (Dept of Osteology) and Andrew P. Currant (Dept of Palaeontology). This work would not have been possible without the kind diligence of Dr Norman Owen-Smith (University of The Witwatersrand), Dr Jeremy Anderson (The Pilanesberg Game Reserve) and Dr Adrian Knott (Natal Parks Board) who provided us with the fetal material.

REFERENCES

BOYDE, A., 1964. *The structure and development of mammalian enamel.* Ph.D. Thesis, University of London.

BOYDE, A., 1967. The development of enamel structure. *Proceedings of the Royal Society of Medicine, 60:* 923–928.

BOYDE, A., 1969. Electron microscopic observation relating to the nature and development of prism decussation in mammalian dental enamel. *Bulletin du Groupement International pour la Recherche Scientifique en Stomatologie, 12:* 151–207.

BOYDE, A., 1974. Real-time stereo TV speed scanning electron microscopy. *Beiträge zur elektronenmikroskopischen Direktabbildung von Oberflächen (Münster), 7:* 221–230.

BOYDE, A., 1976. Enamel structure and cavity margins. *Operative Dentistry, 1:* 13–28.

BOYDE, A. & COWHAM, M., 1980. An alternative method for obtaining converted BSE imaging by specimen biasing in biological SEM. *Scanning Electron Microscopy, 1980, Vol. 1:* 227–232. SEM Inc., AMF O'Hare (Chicago), IL 60666.

BOYDE, A., JONES, S. J. & REYNOLDS, P. S., 1978. Quantitative and qualitative studies of enamel etching with acid and EDTA. *Scanning Electron Microscopy, 1978 Vol. II:* 991–1002. SEM Inc., AMF O'Hare (Chicago), IL 60666.

BOYDE, A. & MARTIN, L. B., 1982. Enamel microstructure determination in hominoid and cercopithecoid primates. *Anatomy and Embryology, 165:* 193–212.

BOYDE, A. & TAMARIN, A., 1984. Improvement to critical point drying technique for SEM. *Scanning, 6:* 30–35.

FORTELIUS, M., 1982. Ecological aspects of dental functional morphology in the Plio-Pleistocene rhinoceroses of Europe. In B. Kurtén (Ed.), *Teeth: Form, Function, and Evolution:* 163–181. New York: Columbia University Press.

FORTELIUS, M., 1984. Vertical decussation of enamel prisms in lophodont ungulates. In R. W. Fearnhead & S. Suga (Eds), *Tooth Enamel IV:* 427–431. Amsterdam: Elsevier.

HOOIJER, D. A. & PATTERSON, B., 1972. Rhinoceroses from the Pliocene of northwestern Kenya. *Bulletin of the Museum of Comparative Zoology, Harvard, 144:* 1–26.

KAWAI, N., 1955. Comparative anatomy of the bands of Schreger. *Okajimas Folia Anatomica Japonica, 27:* 115–131.

OSBORN, H. F., 1903. The extinct rhinoceroses. *Memoirs of the American Museum of Natural History, 1 (3):* 75–164.

PETRAN, M., HADRAVSKY, M., EGGER, M. D. & GALAMBOS, R., 1968. Tandem scanning reflected light microscope. *Journal of the Optical Society of America, 58:* 661–664.

RENSBERGER, J. M., 1983. Effects of enamel structure on wear. *American Journal of Physical Anthropology, 60:* 343–344.

RENSBERGER, J. M. & KOENIGSWALD, W. von, 1980. Functional and phylogenetic interpretation of enamel microstructure in rhinoceroses. *Paleobiology, 6:* 477–495.

RONNHOLM, E., 1962. The amelogenesis of human teeth as revealed by electron microscopy. II. The development of the enamel crystallites. *Journal of Ultrastructure Research, 6:* 249–303.

WOLF, J., 1942. Der Einfluss der Ameloblastenverschiebungen auf die Gestalt und den Verlauf der Schmelzprismen. *Deutsche Zahn-Mund und Kieferheilkunde, 9:* 498–514.

LIST OF ABBREVIATIONS

CPD	Critical point drying/dried
EDJ	Enamel dentine junction
LM	Light microscopy
LS	Longitudinal section or longitudinally sectioned
PLM	Polarized light microscopy
PMMA	Polymethylmethacrylate

SEM	Scanning electron microscopy/microscope
SE	Secondary electron imaging mode
CBSE	Converted backscattered electron imaging mode
BSE	Backscattered electron imaging mode
BSE-ET	Backscattered electron imaging with conventional Everhart Thornley based scintillator
TEM	Transmission electron microscopy
TS	Transverse section or transversely sectioned
TSRLM	Tandem scanning reflected light microscopy/microscope